Eddy Current Array Probe for Metal Additive Manufacturing Imaging

André Barrancos Oliveira
Instituto Superior Técnico
Av. Rovisco Pais 1, 1049 001 Lisbon, Portugal
andre.barrancos@tecnico.ulisboa.pt

***Abstract*—This work presents the development of an eddy current array probe and readout circuits, which will allow online detection of defects layer by layer on metal additive produced parts using Powder Bed Fusion (PBF) technology. This project aims to develop a probe that provides high spatial resolution, spatial coverage, and scalable architecture, enabling a cost-effective modular and extendable probe with 16 sensing/reading coils.**

The first step was to test some coils to help decide which would be the best sensing elements for the final array probe. Also, some initial Printed Circuit Boards (PCB) tests were made to develop an eddy current testing readout with as minimal hardware as possible. In the end, the array probe is presented, which can process the data at high speeds and send the information to a computer to perform the imaging of the test material in real-time.

The array probe has the following specifications: Total size of 80x80 mm; Coils pitch of 5 mm; Total acquisition rate of 20 kSamples/s; Acquisition rate per channel of 5 kSample/s; Demodulation and stimulation frequency up to 1.5 MHz; Internal clock system of the MSP430s of 24 MHz; External oscillator of 24 MHz; Supply voltage from 0 V to 12 V; Total power consumption of 3 W and a total cost of 40 €.

***Index Terms*—Metal Additive Manufacturing, Non-Destructive Testing, Eddy Currents Testing, High Resolution, Minimalist Signal Demodulator.**

I. Introduction

Metal Additive Manufacturing (MAM) is a 3D manufacturing process, where the fabrication of a 3D object is accomplished by joining layers of metal, layer by layer. Nowadays, more and more companies rely on this type of technology to create prototypes and even final products. This type of manufacturing has some advantages, like producing sophisticated objects in a wide range of materials and reducing production setup times compared to other metal manufacturing processes. There are a lot of innovative technologies used in the MAM industry, but this will work will focus only on the Powder Bed Fusion (PBF) technology where laser energy is used to melt and consolidate stacked layers from a base metal powder.

In order to achieve high quality produced parts, it is essential to have high standards of Quality Control (QC) and the ability to detect as much as possible defects while the metal additive parts are being produced. Non-Destructive Testing (NDT) techniques allow to analyze materials without damaging them while detecting any defects or flaws. That is why NDT plays an essential role in the QC that currently exists in the MAM industry since it is vital to evaluate the integrity of the produced parts while tests are made during manufacturing.

In-situ monitoring of PBF produced parts nowadays rely on optical sensors, infrared cameras, thermal cameras and laser-assisted ultrasound tests. These testing technologies have some advantages, like being fine-tuned over the years. However, they require lots of computational power, and most systems do not sample signals at high rates and interpret them immediately (in real-time) [1].

This work aims to use a different approach for the QC of PBF parts. Eddy Currents Testing (ECT) is a popular choice for the characterization of conductive parts within the NDT methods. ECT probes can inspect ferromagnetic and non-ferromagnetic materials with very accurate and high-speed results while being cost-effective. Nevertheless, the main advantage for the MAM industry is that ECT can measure the effective consolidation between successive layers of the test piece. That is why ECT can be an excellent QC alternative to what is currently used in the MAM industry.

II. State Of The Art

Eddy currents phenomenon occurs when a conductive material is close to a varying magnetic field. An electrical voltage is induced on the material, which generates the eddy currents parallel to the magnetic field source and perpendicular to the magnetic induction vector, as an electrical current in a closed loop. In the eddy current probes, a coil generates an alternating magnetic field that induces the eddy currents in the test material [3]. The magnitude of the generated eddy currents is proportional to the magnetic flux change rate, but it's inversely proportional to the material's resistivity [2]. The measurement system senses the magnetic field changes generated by the eddy currents through the same coil or another sensing coil. The voltage output of the measurement system depends on the eddy current's magnetic field variation, which is affected by the distance of the probe to the target material, or if the testing material is different or if the material under test has any discontinuities. In Fig. 1, depicts how eddy currents can be induced by a coil when an Alternate Current (AC) current is flowing.

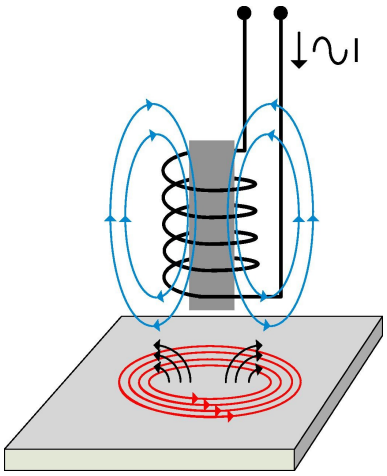

Fig. 1. Eddy currents being induced by a coil. Taken from [3].

III. Coil testing

The first objective of this work was to identify various cheap commercial coils that can be used as sensing elements for the array probe. In this way, hardware had to be developed to do all the required coil testing. In Fig. 2 is shown the support board for the ECF10 module, which is an electronic system able to perform frequency characterization measurements and in Fig 3 is represented the probe used to test different coils. The ECF10 firmware was used in the initial tests, but changes were made to this program not to use the Direct Digital Synthesizer (DDS) and instead to use a square signal generated by the MSP430FR2355 to stimulate the absolute probes. Also, an initial LabView GUI was developed in order to read, write and program the ECF10, and control the CNC machine.

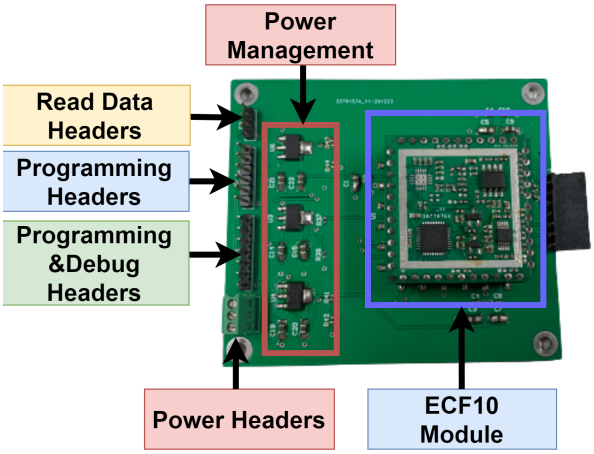

Fig. 2. Developed support board for the ECF10.

Initially, nine coils were tested by making a single scan on a simple defect. In Table. I is shown all the tested coils. Also, preliminary tests were made to understand the system's best operation frequencies, which were determined to be 1 MHz and 1.5 MHz. The initial study concluded that the higher inductance coils were more sensitive in detecting the analyzed defect, and the coils with less than 10 μH had more difficulty detecting the same defect.

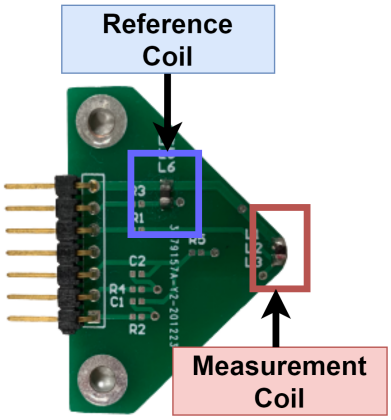

Fig. 3. Developed absolute probe to test different coils.

TABLE I
Initially tested coils.

Tested coils				
Nr	Coils Reference	Ind. [μH]	Shielded?	Coil Type
1	LB2012T101K	100	No	Wirewound
2	L0805C101MPWST	100	Yes	Ferrite Core
3	LB2012T680K	68	Yes	Ferrite Core
4	LBR2012T470K	47	No	Wirewound
5	L0603B4R470MDWFT	47	Yes	Ferrite Core
6	LBMF1608T220K	22	No	Wirewound
7	MLF1608C180KTD25	18	Yes	Ferrite Core
8	LQM18FN100M00D	10	Yes	Ferrite Core
9	MLF1608A3R3JTD25	3.3	Yes	Ferrite Core

Then a more in-depth analysis was made with four coils which had the best results: 100 μH non-shielded, 100 μH shielded, 47 μH non-shielded and a 47 μH shielded coil. In the end, the best results were obtained with the 100 μH shielded.

The results obtained with this coil for an infinite failure can be observed in Fig. 4 a) and Fig. 4 b) for the respective real and imaginary components. The blue and red lines represent, respectively, the response for 1 MHz and 1,5 MHz stimulus.

It was also made a 2D imaging of a hole defect using the 100 μH shielded coil. In Fig. 5 a) and Fig. 5 b) is shown the obtained 2D imaging of a hole defect and the respective real and imaginary component.

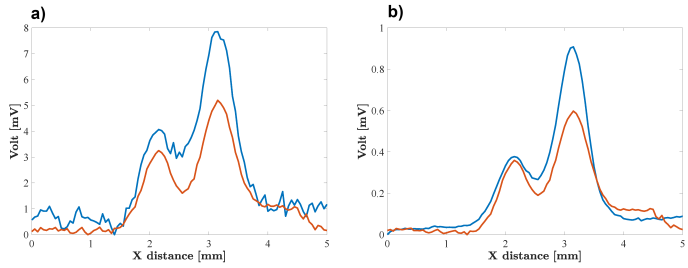

Fig. 4. Real a) and Imaginary b) component of the sensing coil for a 1 MHz (blue) and 1.5 MHz (red) stimulation.

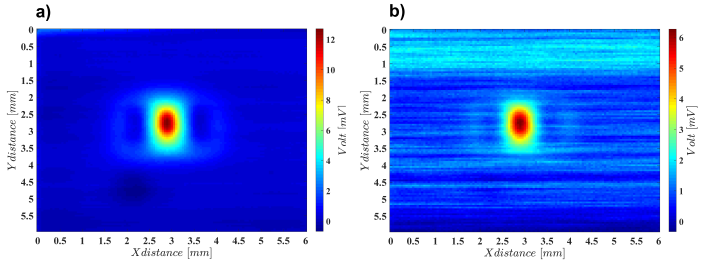

Fig. 5. 2D imaging of the real a) and imaginary b) part component of the sensing coil for a 1MHz stimulation.

IV. One channel probe

Before making the final array probe, a probe was initially made, representing a channel of the final array probe. This probe was developed to reduce as much hardware as possible and thus reducing the costs per channel without compromising the final array probe performance. On Fig. 6 is shown an image of the initial PCB used to make all the necessary tests in order to optimize hardware and hardware costs per channel for the final array probe.

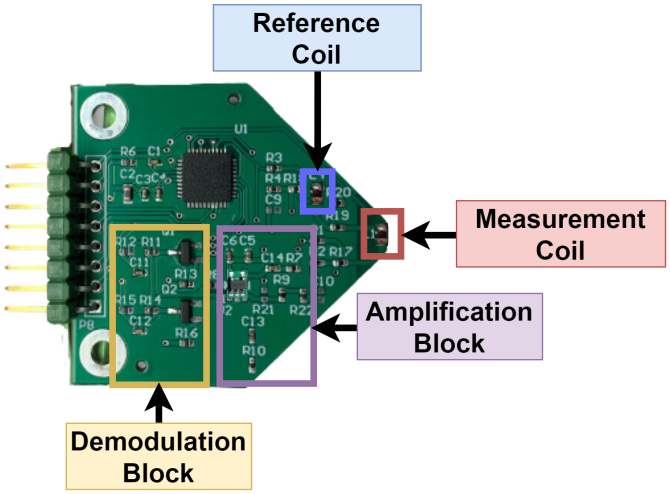

Fig. 6. One channel PCB.

A. Amplification Block Optimization

Initially, the Operational Amplifier (Op-amp) had to be chosen. The initial tests, made in chapter III, were conducted by stimulating the coils with a 1 Mhz or 1.5 Mhz signal and using a programmable gain instrumentation amplifier to amplify the signal's difference between the compensation, and the stimulation coil, with a gain set to 10 or 100. By knowing this information, the operational amplifier for the new PCB should have a gain-Bandwidth Product (GBW) between 15 Mhz (10 x 1.5 Mhz) and 150 Mhz (100 x 1.5 Mhz).

Another requirement for the Op-amp was to have a rail to rail and single-supply operation, so it could be possible to power the amplifier between ground and 5 V. It was also crucial that the chosen Op-amp had a high Slew-Rate (SR), a high Common-mode Rejection Ratio (CMRR) and a low total harmonic distortion. It was decided to use the GS8051 amplifier for the final array probe amongst all the compared Op-amps.

However, after some tests, the results achieved by the amplifier were not being great because the output was constantly saturating. This problem was being caused by the impedance differences between the two input channels of the differential amplifier. This impedance matching is important because when the probe is "resting", without having contact with any material, both signals should cancel each other. By trying to match the input impedances as much as possible is avoided load unbalancing of the measurement and reference coils. In this case, because the input impedance difference between both inputs was very high, different voltage drop showed on each input node of the amplifier, which when amplified lead to the amplifier saturation.

So, in order to solve this problem, the positive channel was connected to a 2,5 V voltage referenced, the voltage divider was set with 24 kΩ resistances, and a capacitor was placed in series for filtering any DC component. The final schematic for the amplification block is shown in Fig.7. The final gain of the differential amplifier is set to 50 and is given by

$$V_{out} = -V_{IN-}\left(\frac{R_5}{R_4}\right) + V_{IN+}\left(\frac{R_3 \parallel R_2}{R_3 \parallel R_2 + R_1}\right)\left(\frac{R_4 + R_5}{R_4}\right), \quad (1)$$

and by having $R_3 \parallel R_2 = R5$ and $R1 = R4$, the amplifier gain equation can be simplified to

$$V_{out} = \frac{R_5}{R_4}\left(V_{ch+} - V_{ch-}\right). \quad (2)$$

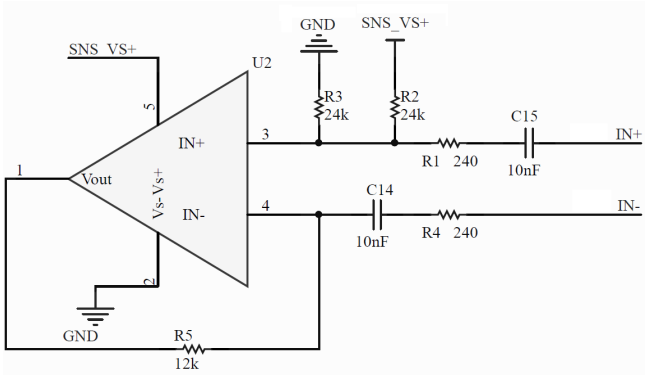

Fig. 7. Schematic for amplification block.

B. Demodulation Block Optimization

Initially, the demodulation block was responsible for the down-conversion of the in-phase and quadrature components of the input signal coming from the amplifier. Thus, two transistors were used where each one had connected a square signal out of phase 90º degrees. This type of demodulation allows the input signal to be mapped on a real-imaginary axis. This information could be helpful, for example, to estimate the probe lift-off, the material's electric conductivity and defects detection. Fig. 8 shows the block's schematic for the IQ demodulator.

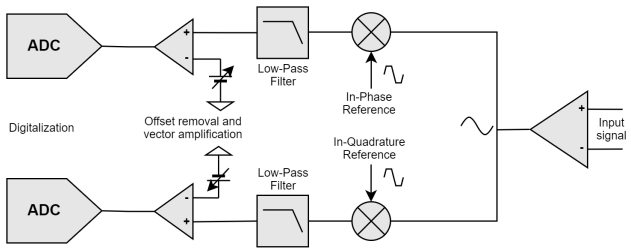

Fig. 8. Block's schematic for the IQ demodulator.

In order to reduce as much as hardware possible in the final probe, only one transistor will be used per demodulation channel, and each channel will only have one low-pass filter set with a cut-off frequency of 1 kHz. Fig. 9 shows the schematic for the demodulation block.

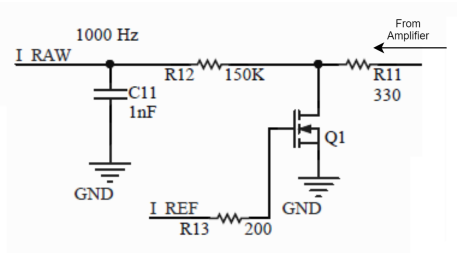

Fig. 9. Schematic for final demodulation block.

When using two transistors it was possible to map the material under test on a real-imaginary axis, like the one represented in Fig. 10.

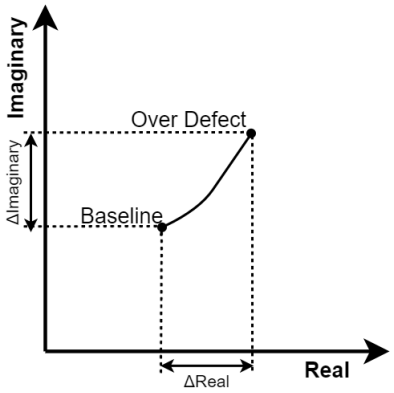

Fig. 10. Defect detection represent on a real and imaginary axis.

However, by demodulating the signal with a single phase reference, some information will be lost. In order to lose the minimum amount of information possible, the phase rotation between the demodulation signal and the stimulation will have to be adjusted to maximize the signal amplitude at the demodulated phase reference, as can be observed in Fig. 11 a), where the axis is rotated. In Fig. 11 b) is represented the amplitude differences of the real and imaginary parts through space. In black is represented the real-imaginary components without axis rotation adjustment and in red with axis rotation. For this example, when the phase rotation occurs, the real part component increases, but the imaginary part gets close to zero.

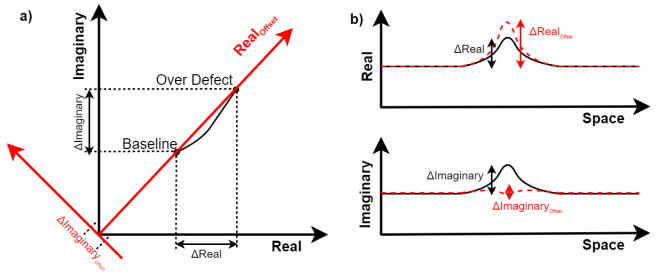

Fig. 11. a) Defect detection represent on a real axis. b) Real-imaginary variations because of axis rotation.

That is why a firmware algorithm was developed to automatically adjust the phase difference between the demodulation and stimulation signal. The algorithm works by initially shifting only the phase of the demodulation signal and acquiring all the data as the phase signal changes on top of an area with no defect. After making all the phase combinations possible, the probe is moved to a place where exists a defect, and the same process is repeated. In the end, the initial acquisitions are compared against the final ones, and the best value for the phase rotation is obtained where was a more considerable difference between acquisitions.

C. SAC configuration

The MSP430 integrates four SACs, and each SAC has inside a low-power Op-amp, a PGA with a gain up to 33, and a 12-bit Digital to Analog Converter (DAC). So, before the demodulated signal gets acquired by the ADC, the signal passes through the SAC. For this project, In order to use four channels per MSP430 is necessary to use the MSP430 SACs in inverting mode as shown in Fig. 12.

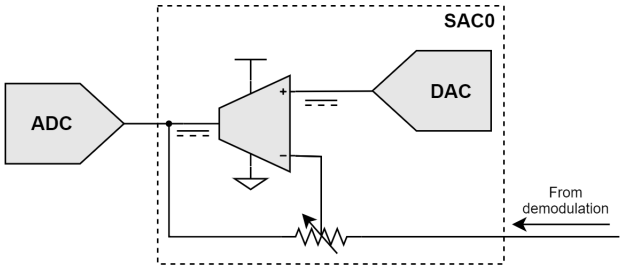

Fig. 12. SAC in inverting mode.

By choosing this mode, the input signal is initially amplified by the PGA where the user digitally controls the gain up to 33x. Then, the Op-amp amplifies the signal difference between the DAC and the amplified input signal's. By making the offset removal, the signal's difference can be more amplified, which allows to explore better the dynamic range of the ADC.

V. The Array Probe

The objective is to develop a probe that is cost-effective and capable of being replicated by integrating multiple coils side by side and able to measure and detect defects on the materials under testing. For this project, only one module was developed. However, the future objective would be to interleave and offset array probes to reduce the space between coils to increase resolution and increase the analysis area by joining array probes side by side. The final array probe PCB is shown in Fig. 13 and in Table II is shown the probe specifications. The probe is divided into five blocks: the power management; the probe channels, which consists of sixteen channels; the processing block, which is composed of four microcontrollers and the FTDI FT4232 mini-module, which is a Universal Serial Bus (USB) to Universal Asynchronous Receiver-Transmitter (UART) converter; the oscillator; and the programming/debugging headers.

TABLE II
Probe Specifications

Probe size	80x80mm
Coils pitch	5mm
Number of coils	32
Acquisition rate	20 kSamples/s
Acquisition rate per channel	5 kSamples/s
Demodulation and stimulation frequency	Up to 1.5 MHz
Internal clock and external oscillator	24 MHz
Supply voltage	0-12V
Power consumption	3 W

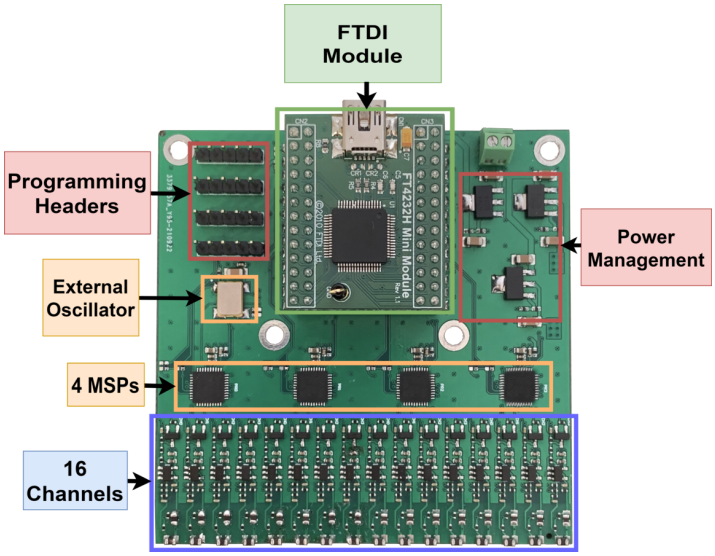

Fig. 13. Array probe PCB.

VI. Hardware

A. Probe Sensors

The topology used for the sensor part was the absolute probe topology. This topology was chosen because it is intended to use the probe to measure conductivity and detect defects. The reference coil's signal is subtracted with the measurement coil's signal before amplifying the signal. Thus the variations at the output of the amplifier caused by the conductivity will be more significant than without a reference coil. In fig. 14 is shown the schematic for the sensors.

One of the pads of the coils is connected to the MSP430, which generates Pulse Width Modulation (PWM) to drive the coils, and another coils pad is connected to the ground. The resistance in series is used to conditioning the current coming from the MSP430.

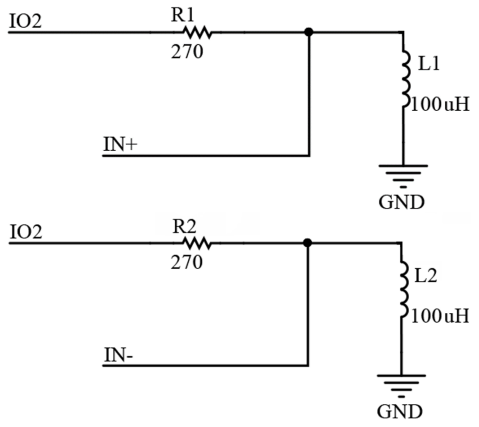

Fig. 14. Respective schematics for the stimulation and compensation sensors.

B. Probe channels

The array probe consists of sixteen channels. Each channel is composed of two coils, one compensation and one stimulation/sensing coil, a differential amplifier with a gain set to 50, a transistor to demodulate the Op-amp signal difference, and a low pass filter set with a cut-off frequency of 1 KHz.

For the final array probe, it was decided to use the 100 μH shielded coils due to their better sensibility in detecting and reconstructing the defects analysed in chapter III.

C. Processing Block

Four microcontrollers and the FTDI mini-module FT4232 constitute the processing block. Each microcontroller is responsible for acquiring the data from four channels, in a total of sixteen channels. Each one of the microcontrollers is responsible for stimulating four channels, controlling the demodulation signals and obtaining each channel's information. After acquiring the data, the data is sent to the FT4232 mini-module. The FT4232 is responsible for receiving all the data from the four microcontrollers. The communication between the four MSP430FR2355 and the FTDI mini-module is achieved by using the UART communication protocol. After receiving all the information, the FT4232 mini-module sends the information to the computer by USB using the USB protocol communication.

D. External Oscillator

For the final PCB, there are four microcontrollers. So is essential that all the MSP430 have the demodulation and stimulation synchronized between them. Otherwise, if independent demodulation and stimulation sources were used, their frequency differences and drift could result in cross-channel interferences. Those interferences would result in a low-frequency beating, whose frequency would equal the frequency difference between adjacent channels. So an external oscillator was used with a frequency of 24 MHz to sync the stimulation and demodulation between MSP430.

E. Power Management

The array probe has an input supply voltage of 0 V to 12 V, connected to three linear voltage regulators, LM317. One of the voltage regulators converts the input voltage to 3.3 V, and the other two convert to 5 V. These two voltage regulators supply 5 V because one of the 5 V supplies the digital part of the probe, which is the FTDI mini-module, and the other 5 V supplies the analogue part of the circuit, in this case, the Op-amps. These 5 V supply voltages are decoupled in order to create fewer interferences in one another. The 3.3 V supplies the four MSP430FR2355. The final system has a power consumption of 3 W and each MSP430 a power consumption of 200 mW.

VII. Firmware

A. Probe excitation and demodulation

A square signal is generated by the MSP430 using the internal timers of the microcontroller. One-timer is used for each compensation and stimulation coils, and another timer is connected to the four transistors' gates.

The square signal is generated by programming the registers CCR0, CCR1 and CCR2. The first register (CCR0) defines the value until the timer counts, completing an entire cycle. The other two registers (CCR1 and CCR2) holds the value when the square signal output changes from high to low. The following formula obtains the frequency code that is saved in the register CCR0

$$Freq_{code} = \frac{Freq_{clock}}{Freq_{out}} - 1. \tag{3}$$

For our example, the square signal is set to 1 MHz, corresponding to the variable Freqpwm, and the clock source is set to 24 MHz, corresponding to the variable $Freq_{clock}$. In this case, the value saved to the register CCR0 would be 23, and in the other two registers to have two square signals in phase, the value saved would be half of the $Freq_{code}$, which would be 12. To have two square signals out of phase by 90º degrees, CCR0 would equal 23, CCR1 equal 12, and CCR2 equal 0.

B. Configuring the ADC

The MSP430 only has one ADC, and the ADC is responsible for digitally convert four channels. The MSP430's ADC can be set to 10 or 12-bit analogue-to-digital conversions and have a maximum sampling rate of 200 kSamples/s. The ADC is set to work on single-channel conversion, converting each channel one by one with 12-bit conversions. The interrupt to acquire each acquisition was triggered automatically over hardware every time TB1 reached the maximum count value. If in alternative, any software mechanism involving the CPU intervention was used, it would not be possible to ensure that the sampling instants would remain exactly equally spaced and coherent with the excitation signal. The timer TB1 was set with a frequency of 20 kHz. This means that the ADC has a sampling rate of 20 kSamples/s, which means a sampling rate

of 5 kSamples/s per channel. The ADC also has a reference voltage of 2.5 V.

C. Moving Average Filter

A moving average filter was programmed to filter the acquisitions. Each MSP430 has four buffers implemented to write each channels acquisitions to the respective buffer. When the buffers are full, it starts to overwrite the data from the initial to the last position of the buffers. When the user wants to read the acquired data, a command is sent to the microcontroller. After that, all the buffers positions are summed and sent to the computer and, then the LabVIEW program makes the average of the sums, filtering all possible outliers.

In order to have a fast system, when the system is turned one, the ADC starts to make acquisitions and writes the information to the buffer without the user input. This way, when the user sends a command requesting for the acquisitions, all the data contained in the buffers is sent, making the start and stop commands obsolete.

D. Protocol communication

The communication between the FTDI module and the four MSP430 was made by using the UART port. In Table. III is shown the structure of the data package for the communication between the MSP430, the FTDI module, and subsequently the PC.

TABLE III
UART PACKAGE STRUCTURE

Data Pack structure	
Command code	1 byte
Value send	4 bytes
Data size	1 byte
Data	Up to 256 bytes
CRC code	1 byte
End of package code	1byte

The first command defines which function will be executed by the MSP430, and the second command is the value written onto the microcontroller used by the command function. The data command corresponds to the data sent from the MSP430 to the FTDI module, but the data size has to be defined with the data size command. The CRC code command is used to verify if the data was correctly sent and received, and the last command is used to tell the microcontroller and the PC that the end of the package has been reached.

The following shows the five commands used to communicate with the MSP430 and the respective hexadecimal code.

- ***Read command*** (0x20) is used to retrieve the data from the MSP430;
- ***Frequency command*** (0x32) is used to adjust the stimulation and demodulation frequency, and frequency up to 1.5 MHz can be set;
- ***Digital gain command*** (0x34) sets the gain for the internals PGA of the MSP430, where a maximum gain of 33x can be set;
- ***Calibration command*** (0x38) is used to adjust the phases between the demodulation and stimulation signals to make the probe more sensitive in detecting defects.
- ***Compensation command*** (0x3A) is used to compensate each probe channel by adjusting the DAC's value of the microcontroller so that the converted digital amplitude in each channel for the initial position is close to 2048. This way, when the channels detect some defect or interferences, the converted digital value will vary between 0 to 4096, being the converted value 2048 a position without defects. Summarizing this command is used to set the initial position of the array probe as the comparison point for the other points of the test material that will be analyzed.

VIII. User interface

A PC application was developed to communicate with the array probe and the CNC machine using LabVIEW 2020. The GUI presented in Fig. 15 allows the user to configure the array probe parameters like the stimulation and demodulation frequency and the PGA gain inside the MSP430, and there is also the Calibration and Compensation buttons. All the commands were explained in more detail in chapter VII-D.

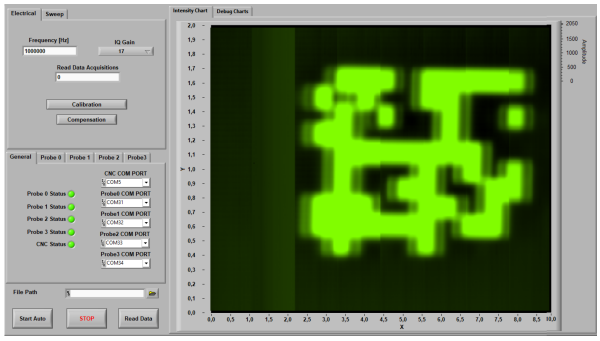

Fig. 15. LabVIEW GUI to communicate with the array probe.

The GUI also lets the user check the status of the array probe and the CNC machine in case some error occurs during the programming and use of the probe and CNC. Also, if a file path is given, the acquired data can be exported to a .mat file.

The developed Labview program also lets the user control the array probe manually or automatically. On the manual mode, the user only has to put the number of acquisitions needed and press the "Read Data" button.

For the automatic mode, the user has to use the interface CNC interface. The user has to give the X-Y travel distance, the number of steps for each axis, and the X-Y direction, and so an intensity chart from the analysed material will be obtained by pre-programming this information and pressing the "Start-Auto button". It is also possible only to move the CNC machine using the arrow keys.

IX. Results

The initial tests to decide which was the best sensing element for the array probe led to the choice of the 100 μH shielded coils. For all the tests conducted it was used, a stimulation and demodulation frequency of 1MHz, a digital gain of 17, and an analogue gain of 50.

To simulate the metal layers produced by a PBF machine, it was used some patterns that were developed in another project. Each pattern is square PCB with 100mm side. The less dark blue zones of the PCBs are the areas where exists metal and the darker zones are the zones where the metal was removed. Each PCB has a 1mm metal layer thickness. It was also analysed a drilled hole defect with a 0.8mm diameter. In Fig. 16 are shown all the analysed patterns by the array probe.

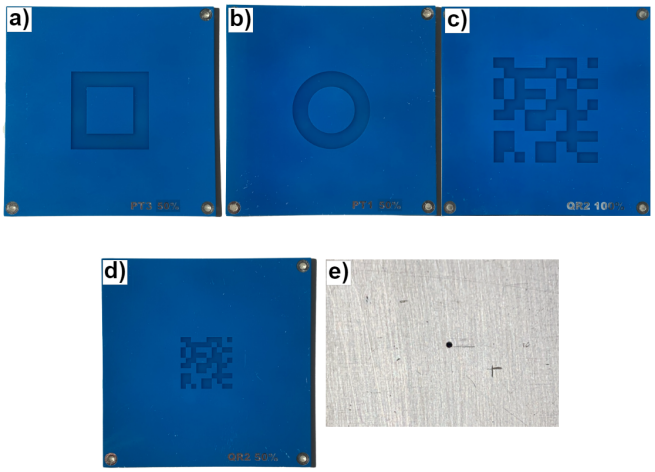

Fig. 16. Analyzed patterns and hole defect by the array probe.

The first pattern analyzed was the square pattern. The biggest square pattern has a side of 25x25mm, and the inside square has a side of 15mm. In Fig. 17 is represented the 2D imaging obtained by the array probe and in Fig. 16 a) the respective pattern. The reconstructed square has a more rectangle shape because the probe response is not omnidirectional, and so the reconstructed pattern stretches to the X direction. The square pattern has a distance between metals of 5mm, and the reconstructed pattern has a respective distance of 4.8mm and 4mm, as can be observed in Fig. 17.

The second pattern analyzed was the circle pattern. The biggest circle pattern has a 25mm diameter, and the inside circle has a diameter of 15mm, which means a distance between metals also of 5mm. Fig. 18 shows the circle 2D imaging and in Fig. 16 b) the respective pattern. The reconstructed circle also has a more oval shape also, due to the probe response being not omnidirectional.

From the analysis of the two 2D imaging figures, a pattern starts to be noticed, which is the colour variation between different channels. Some channels are more sensitive than others because of the coils lift-off due to difficulties when hand-soldering the coils, making some coils closer or further away from the test material. The redder zones are the zones

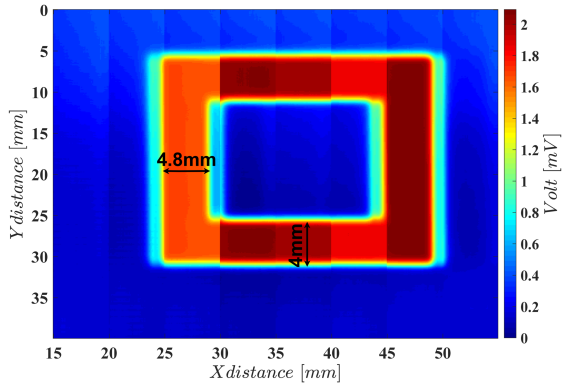

Fig. 17. 2D imaging of a square pattern.

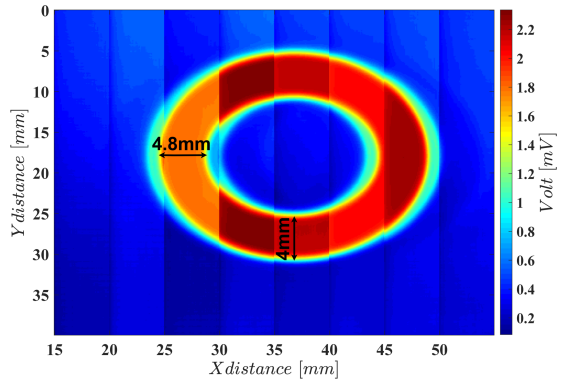

Fig. 18. 2D imaging of the circle pattern.

where the coils are closer to the test material. In Fig. 19, it can be observed that some channels coils are a bit closer and others farther away from the test material.

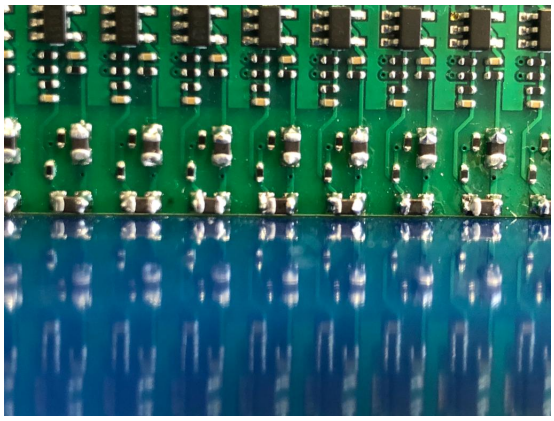

Fig. 19. Misaligned coils.

A sensitivity offset value can be given to each channel to solve this problem to compensate for the distance between

coils to the test material. Eventually, this problem could be solved by using an automated soldering machine. However, even if that could not solve all the channels offset, a simple calibration process could solve it by using a known test material and then fine-tuning each sensitive element manually or automatically for that known material. In Fig. 20 is shown the already analyzed patterns but with a compensation value on the post-processing data for each channel.

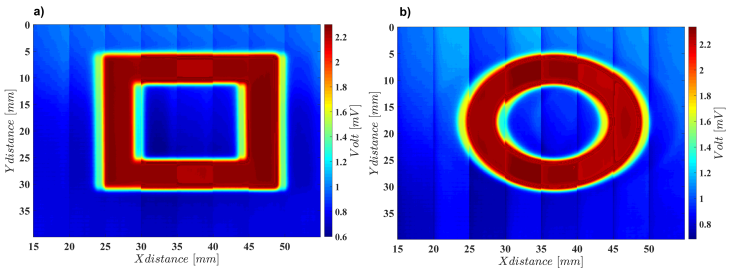

Fig. 20. Square and circle 2D imaging with channel compensation.

The third pattern analyzed was a squared QR code with a 50mm side, with square patterns as small as 5mm. In Fig. 21 is the obtained 2D imaging and Fig. 16 c) the scanned pattern. This pattern was used to test if the array probe could detect patterns close to each other. By analyzing the 2D imaging image, it is possible to observe that the array probe detects well the patterns, but the metal layers between patterns are less noted.

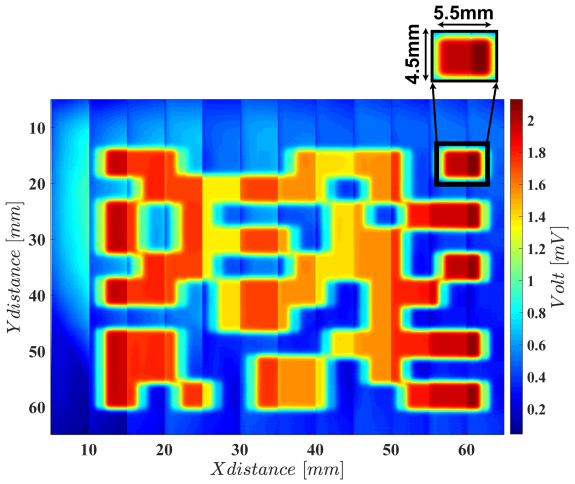

Fig. 21. Bigger QR code 2D imaging.

A fourth pattern with the same squared QR code but half of the size was analyzed to check if the probe could still detect the small patterns with a size of 2.5mm. In Fig. 22 is shown the small QR code 2D imaging and the respective pattern is shown in Fig. 16 d). The test shows that the scanned patterns still have a good resolution and have almost the same size as the analyzed material. One thing noticed was that the small metal layers, between patterns, are still even less noted than in the previous scan. This was expected because the magnetic field generated by the coils generates small eddy currents on the metal, which creates a small magnetic field detected by the measurement coil. So the smaller metal zones are less darker, making the small metal zones less visible on the 2d imaging.

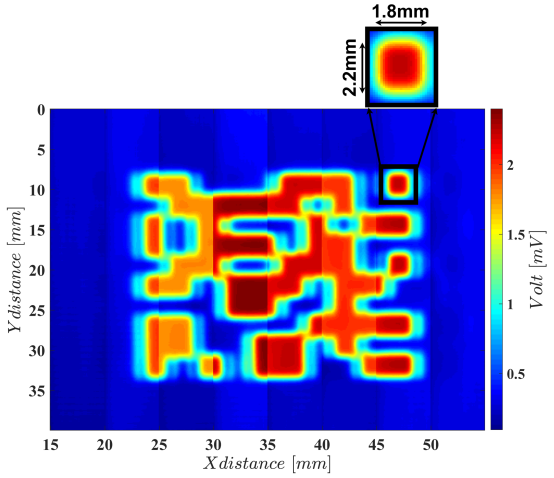

Fig. 22. Smaller QR code 2D imaging.

The final test was made in an even smaller defect. This time the defect was a hole with a 0.8mm diameter. In Fig. 23 is shown the 2D imaging of the hole and in In Fig. 16 e) the respective hole.

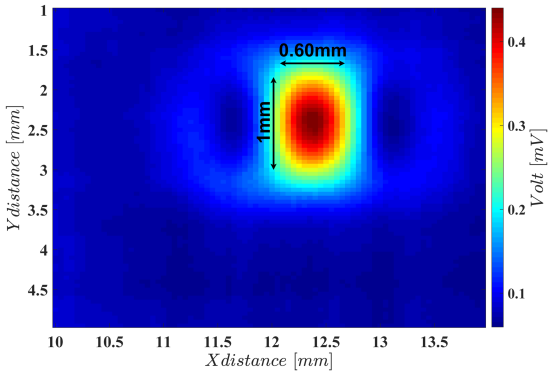

Fig. 23. Hole defect 2D imaging.

From the 2D imaging, it can be observed that the error is more significant compared to other bigger analyze. However, the approximation distances obtained are still a good approximation.

X. Conclusions

This project presented a system based on the ECT method for the QC of the in-situ monitoring, layer by layer, of manufactured pieces using PBF technology, which is a manufacturing process on the MAM industry.

In this work, coils were initially tested to decide which were the best sensing elements for the final array probe. After that, some PCBs were developed to reduce as much hardware as possible and optimize the costs per channel for the final array probe. In the end, the developed array probe has sixteen channels for stimulation and reading and a size of 8x8cm, which means the final array probe can analyze materials in one sweep of 8 cm and all of that with a minimal cost of 40€. In theory, if the user would like to have a more extensive coverage area, it would only need to put probes side by side, and if it would want to increase the resolution per sweep, it would only have to put the PCBs interleaved.

In the end, the results were the expected. The array probe scanned different types of patterns and defects of a size as small as 0.8mm. The worst part was the time that the CNC machine would take to scan a pattern. The biggest pattern with a size of 8x8cm with a step of 0.1mm would take almost three hours to be thoroughly scanned. So due to that, the future work suggestions are focused on improving faster readouts from the sensors and improving the array probe's accuracy and are as follows.

- Make a control system that can move the CNC machine and acquire data at the same time in order to have a faster system;
- Evaluate different algorithms for the inspected surface reconstruction from the probe provided data. Specifically, the use of Deep-Learning may provide interesting results while dealing with the complex relation between the surface features and the ECT imaging data;
- Ensure the necessary high-level synchronization with other probe modules, for instance, providing an input for a higher level clock instance;
- Define and implement a faster digital readout architecture for several microcontroller instances. For example, using a Field Programmable Gate Array (FPGA) to aggregate and dispatch through USB the output data from multiple microcontrollers connected through a Serial Peripheral Interface (SPI) bus;
- Evaluate other eddy current sensing strategies as the use of commercial magneto-resistive sensors as the Crocus Technology CT-100;
- Evaluate the probe on real PBF produced parts and specifically during the processing of the successive layers.

REFERENCES

[1] S. Clijsters, T. Craeghs, S. Buls, K. Kempen, J.P. Kruth, "In situ quality control of the selective laser melting processing a high-speed, real-time melt pool monitoring system", Int J Adv. Manuf Technol, vol. 75, pp. 1089-1101, 2014.

[2] https://en.wikipedia.org/wiki/Eddy-current_testing, last access on November 1th 2021.

[3] N. Rodrigues, L. Rosado, P. Ramos, "A portable embedded contactless system for the measurement of metallic material conductivity and lift-off", Measurement, vol. 111, December 2017.